Complex [40]Ar/[39]Ar age spectra from low metamorphic grade rocks: resolving the input of detrital and metamorphic components in a case study from the Delamerian Orogen

Anthony Reid[1, 2], Marnie Forster[3], Wolfgang Preiss[1, 2], Alicia Caruso[1], Stacey Curtis[1,4], Tom Wise[1], Naina
5 Goswami[3]

[1]Geological Survey of South Australia, Department of State Development, GPO Box 320, Adelaide, SA 5001, Australia
[2]Department of Earth Sciences, School of Physical Sciences, University of Adelaide, SA 5005, Australia
[3]Mineral Exploration Cooperative Research Centre, Research School of Earth Sciences, The Australian National University,
Canberra, ACT 2601, Australia.
10 [4]Mineral Exploration Cooperative Research Centre, STEM, University of South Australia, Mawson Lakes, Australia

Correspondence to: Anthony Reid (anthony.reid@sa.gov.au)

Abstract. Low metamorphic grade rocks contain both detrital minerals and minerals newly grown or partly recrystallised
during diagenesis and metamorphism. However, rocks such as these typically yield complex [40]Ar/[39]Ar age spectra that can be
difficult to interpret. In this study, we have analysed a suite of variably deformed rocks from a region of low metamorphic
15 grade within the c. 514 – 490 Ma Delamerian Orogen, South Australia. The samples analysed range from siltstone and shale
to phyllite and all contain either muscovite or phengite determined by hyperspectral mineralogical characterisation. Furnace
step heating [40]Ar/[39]Ar analysis produced complex apparent age spectra with multiple age components. Using the concept of
asymptotes that define minimum and maximum ages for different components, we interpret the age spectra to preserve a range
of detrital mineral ages, along with younger components related to either cooling or deformation- induced recrystallisation.
20 Two samples contain Mesoproterozoic detrital age components, up to c. 1170 Ma, while the c. 515 Ma Heatherdale Shale
which has both c. 566 Ma and c. 530 Ma detrital components. All samples contain younger lower (younger) asymptotes in the
age spectra defined from multiple heating steps that range from c. 476 to c. 460 Ma. One interpretation of these younger ages
is that they are caused by post-metamorphic cooling. However, the shape of the age spectra and the degree of deformation in
the phyllites suggest the ages may record recrystallisation of detrital minerals and/or new mica growth during deformation.
25 Potentially these c. 476 to c. 460 Ma ages suggest deformation in the upper portion of the orogen was facilitated by movement
along regional faults and shear zones up to around 20 million years after the cessation of deformation in the high-metamorphic
grade regions of the Delamerian Orogen.

1 Introduction

Low metamorphic grade rocks are a common feature in most orogens as they constitute the upper portion of an orogen, distal
30 to more deeply exhumed high metamorphic grade core. In many orogens, low metamorphic grade rocks comprise the vast bulk

of the surface exposure, and hence are potentially a significant source of information on the orogenic process. However, most studies into the rates and timing of orogenesis concentrate on the high metamorphic grade sections of orogens because high temperature minerals are either completely newly grown during orogenesis, or at least, isotopically reset. Low metamorphic grade rocks in contrast, typically comprise a mixture of detrital minerals and newly grown diagenetic or metamorphic minerals

35 (e.g. Dunlap et al., 1991; Cosca et al., 1992; Kirschner et al., 2003; Chan et al., 2000; Fergusson and Phillips, 2001; Dallmeyer and Takasu, 1992; Dallmeyer et al., 1988; Clauer, 2013). As a result, and especially when dealing with fine-grained, low-metamorphic grade rocks, it can be difficult to separate detrital from metamorphic signals in isotopic analysis of whole rock samples (see also Phillips et al., 2012).

40 In this paper we show that $^{40}Ar/^{39}Ar$ furnace analysis of low metamorphic grade rocks can provide information on the possible detrital component of these rocks, as well as yield insights into the timing of orogenic activity. This approach can be viewed as complimentary to $^{40}Ar/^{39}Ar$ dating low metamorphic grade rock fabrics using in situ laser microprobe methods (e.g. Chan et al., 2000; Kirkland et al., 2008). Our field area, the Mount Lofty Ranges of South Australia, provides an ideal setting with which to investigate low metamorphic grade rocks, because of the extensive exposure of Neoproterozoic to Cambrian

45 metasedimentary rocks in this part of the Delamerian Orogen. The results identify Mesoproterozoic detrital components along with Cambro-Ordovician age populations related to cooling or deformation.

2 Geological setting

The Delamerian Orogen formed on the eastern proto-Pacifc margin of Gondwana in the Late Cambrian to early Ordovician and is part of the family of orogens developed during amalgamation of Gondwana (Fig. 1; Preiss, 1995; Foden et al., 2006;

50 Cawood, 2005; Glen and Cooper, 2021). The Delamerian Orogeny deformed Neoproterozoic to early Cambrian rocks of the Adelaide Superbasin, including the early Cambrian Kanmantoo Group and Normanville Groups. The Neoproterozoic stratigraphy includes the Burra, Umberatana and Wilpena Groups, which were deposited in a series of rift and sag basins associated with the breakup of the supercontinent Rodinia (Fig. 2; Preiss, 2000; Lloyd et al., 2020; Flottmann et al., 1998; Preiss, 1987). Deposition of the Kanmantoo and Normanville groups is contemporaneous with the earliest arc magmatism

55 along the Gondwanan subduction margin to the east of the Delamerian Orogen (Betts et al., 2018). The Delamerian Orogen is a fold-thrust belt in which the rift complex units, as well as parts of the underlying Paleo-Mesoproterozoic basement, were thrust towards the Archean-Mesoproterozoic Gawler Craton. A series of western frontal thrusts separate the strongly folded and faulted rocks from the Torrens Hinge Zone, a zone of transition between the thick, highly deformed succession and the platform sediments of the Stuart Shelf that overlie the basement of the Gawler Craton to the west (Fig. 3; e.g. Flottmann and

60 James, 1997). There is no compelling evidence of deformation, other than rifting, between the Neoproterozoic and Cambrian, and both successions have been deformed and metamorphosed together. Metamorphic isograds cross some stratigraphic boundaries, especially within the Kanmantoo Group, but some others coincide with major faults (Fig. 3; Offler and Fleming,

1968; Mancktelow, 1990; Dymoke and Sandiford, 1992). The lowest metamorphic grade regions occur along the western edge of the orogen, where weakly cleaved rocks contain metamorphic chlorite defining a chlorite-zone (Fig. 3), from where several
65   samples analysed in this study were derived. Peak metamorphic conditions of ~3-5 kbar and 550-650 °C occur in a migmatite-grade zone in the east of the orogen, demonstrating regional metamorphism low-pressure, medium- to high-temperature in style (Dymoke and Sandiford, 1992; Preiss, 1995). Deformation and metamorphism began at c. 514 Ma with emplacement of early, syn-tectonic granite (Foden et al., 1999). A belt of, high-level, undeformed granites cut major structures in the eastern parts of the orogen formed at c. 490 Ma, suggesting that the entire orogenic cycle occurred over an approximately ~24 million
70   year period in the late Cambrian (Foden et al., 2006).

The few available ^{40}Ar/^{39}Ar analyses from the Delamerian Orogen have mostly been interpreted to record post-peak metamorphic cooling (Foden et al., 2020; Foden et al., 2006; Turner et al., 1996). Laser ^{40}Ar/^{39}Ar analyses of syn-kinematic muscovite from folded schists in the Delamerian Orogen yielded a plateau age of 502 ± 4 Ma, interpreted to record cooling
75   subsequent to D_1 thrusting (Foden et al., 2020). Laser ^{40}Ar/^{39}Ar analyses of biotite and hornblende from syn-kinematic, largely I-type granites and from country rocks yield ages that range from c. 498 – 480 Ma (Turner et al., 1996), which broadly corresponds to the timing of intrusion of late-kinematic to post-kinematic granites and mafic rocks. Turner et al. (1996) interpreted the orogen to have cooled below ~300 °C by c. 480 Ma. This is consistent with a muscovite ^{40}Ar/^{39}Ar age of 478 ± 2 Ma from a high-level post-tectonic pegmatite (Burtt and Phillips, 2003). Importantly, however, the currently available
80   ^{40}Ar/^{39}Ar data are all from rocks within the high metamorphic grade portions of the orogen. There is no ^{40}Ar/^{39}Ar data published from the lower metamorphic grade regions of the Delamerian Orogen.
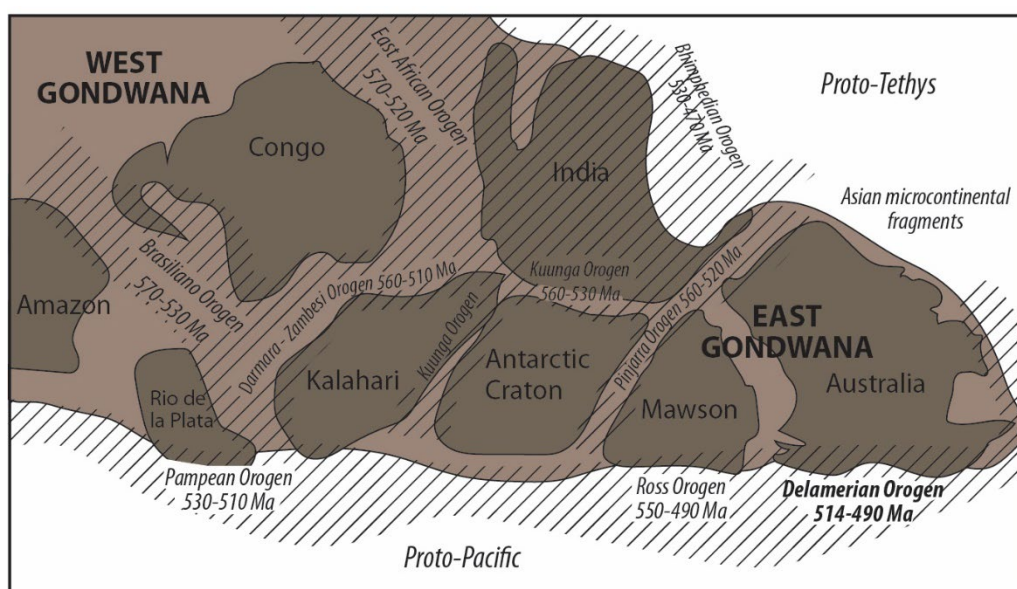
Figure 1. Location of the Delamerian Orogen with respect to east Gondwanan terranes. Modified from Cawood et al. (2007).

DEM 205463-057

0   25   50 Kilometers

GDA2020 Zone 54
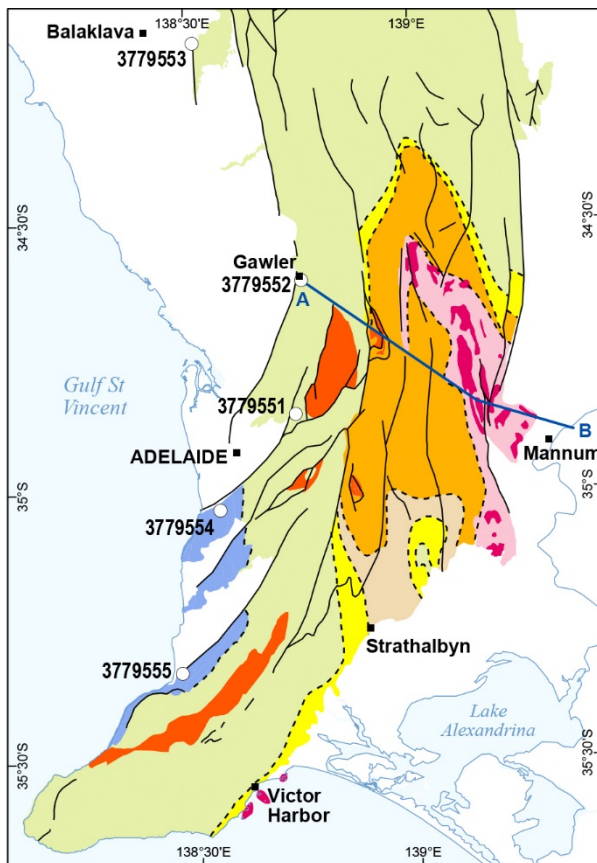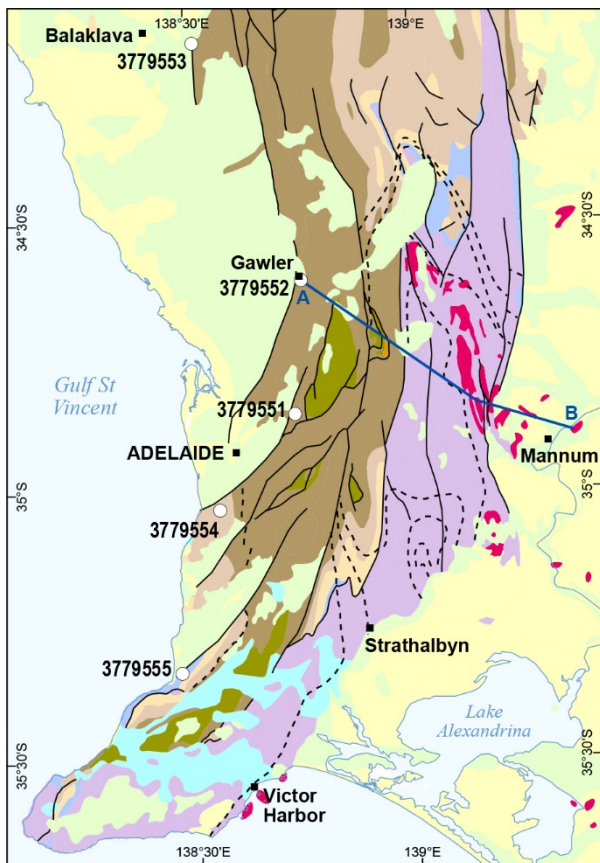
2 000 000 surface geology

CENOZOIC
- Pleistocene–Holocene
- Palaeogene–Neogene

CARBONIFEROUS-PERMIAN
- Cape Jervis Formation

CAMBRIAN-ORDOVICIAN
- Granitoid rock of the Delamerian Orogeny

CAMBRIAN
- Kanmantoo Group
- Normanville Group

NEOPROTEROZOIC
- Wilpena Group
- Umberatana Group
- Burra Group
- Mount Crawford Granite Gneiss

PALAEOPROTEROZOIC
- Barossa Complex
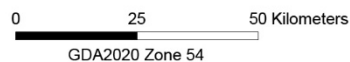
Delamerian metamorphic zones
- Chlorite zone
- Biotite zone
- Barossa Complex amphibolite facies, retrogressed to greenschist facies
- Andalusite-straurolite zone
- Fibrolite zone
- Prismatic sillmanite zone
- Migmatite zone
- Delamerian granite

○ Sample locations

—— Location of Gawler-Mannum cross-section of Figure 3

—— Fault position accurate

----- Metamorphic isograd (non-faulted)

Figure 2: Geology of the Mt Lofty Ranges, part of the Delamerian Orogen, showing location of samples analysed in this study. (a) 1:2 million scale South Australian state-wide geology dataset. (b) Delamerian metamorphic isograds of the Mt Lofty Ranges (after Offler and Fleming, 1968; Mancktelow, 1990; Dymoke and Sandiford, 1992; Preiss, 1995).

90
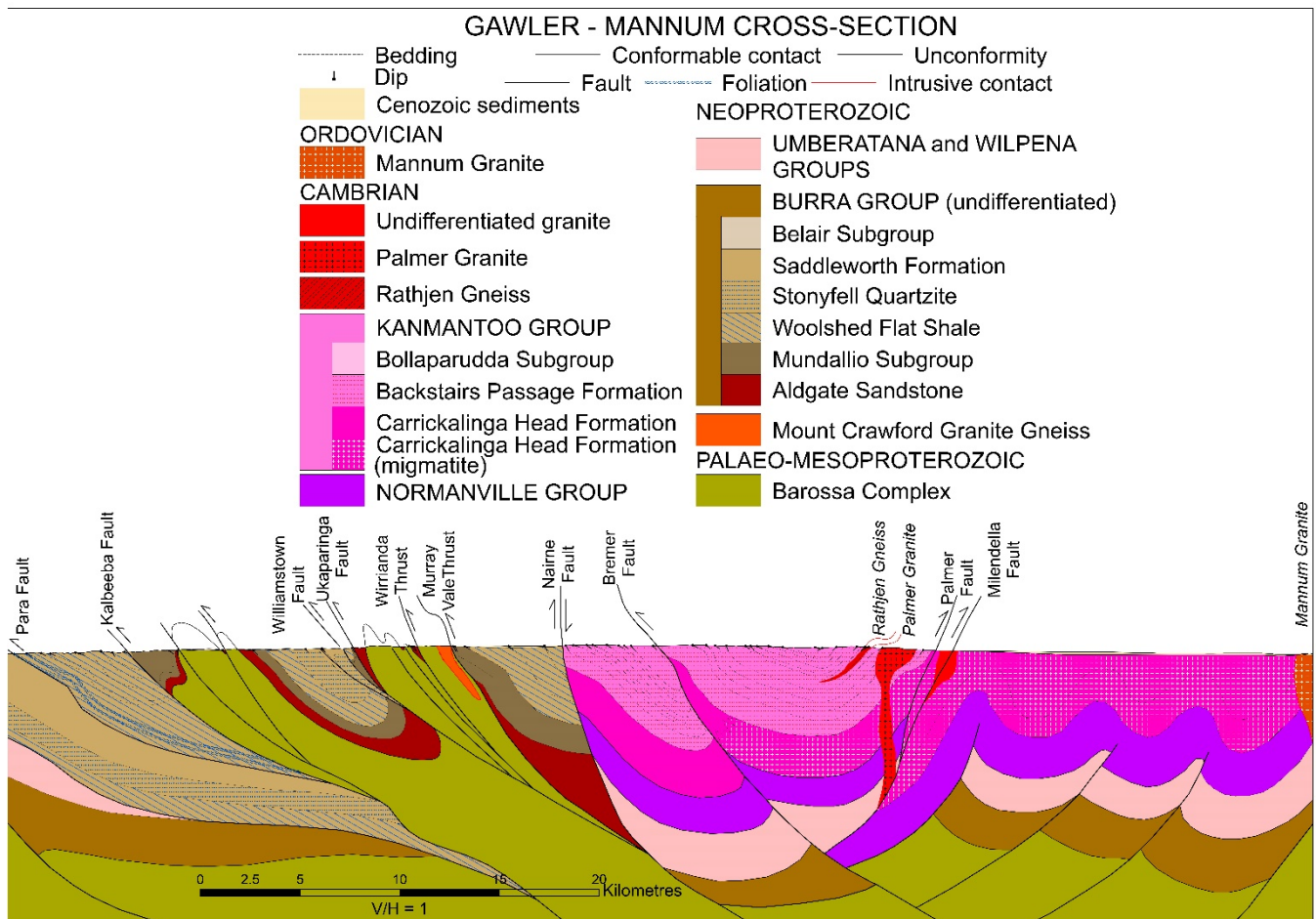
Figure 3. Interpretative cross-section across the southern Delamerian Orogen from Gawler to Mannum. Topographic profile and surface geology, including dip of structural elements, are well constrained from previous mapping, but their extrapolation at depth in this diagram is more speculative. The left-hand portion of the cross-section illustrates the westerly vergence of the major structures in the western, low metamorphic grade zones, and the involvement of the basement. Many of the faults originated as extensional faults in the basement as a result of Neoproterozoic and Cambrian rifting. Of the mapped major faults, the Para, Kalbeeba. Williamstown, Bremer, Palmer and Milendella faults all display compressional neotectonic reactivation. The Nairne Fault differs from other faults in being a ?late Delamerian normal reactivation of a Cambrian extensional fault, and locally forms the western boundary of the Kanmantoo Trough. Metamorphic grade jumps from greenschist facies to sillimanite grade across the Williamstown Fault, while migmatite is widely developed in the oldest formation of the Kanmantoo Group. Geology beneath the Kanmantoo Group is schematic only. Location of cross section shown in Figure 2, A-B.

95

100

105

3 Sample descriptions

To test if the Delamerian Orogen did end at c. 480 Ma across the entire region, we have sampled rocks within the biotite and chlorite metamorphic zones of the orogen and analysed them using whole rock $^{40}Ar/^{39}Ar$ methods (Table 1; Fig. 2). As many

110 of these samples are very fine-grained we have undertaken mineralogical characterization using hyperspectral imaging with Hylogger 3^{TM} instrumentation (Schodlok et al., 2016) at the South Australian Drill Core Reference Library, Adelaide. Full details of Hylogger 3^{TM} methodology and mineralogical composition of samples from this study are given in Appendix A.

Sample 3779553 is a phyllite in the lower part of the Burra Group exposed east of the township of Balaklava. At this locality,

115 the phyllite is a deformed thrust sheet with a low-angle tectonic foliation that sits in the hanging wall of a regional fault (Redbanks Fault). The foliation dips west at a very shallow angle suggesting that it has been gently folded in a hanging-wall antiform (Preiss, 2019). A down-dip mineral lineation is overprinted by mm-scale crenulations trending ~340° (Fig. 4a). This locality is near the western-most extent of the Delamerian Orogen. Mineralogically this sample comprises chlorite (FeMg- and Mg-rich), phengitic white mica, albite, muscovite and quartz identified across both the Shortwave Infrared (SWIR) and

120 Thermal Infrared (TIR) wavelength ranges (Appendix A).

Sample 3779552 is a phyllitic schist from within an east-dipping thrust sheet located stratigraphically within the Woolshed Flat Shale, at the southern outskirts of the township of Gawler. The sample is phyllitic, fine-grained, with intense schistosity, and has a well-developed, down-dip mineral lineation (Fig. 4b). The locality also has evidence for boudinaged quartz veins

125 sub-parallel to the foliation, and local mm- to cm-scale quartz veins that cut the foliation. Interpreted SWIR mineralogy for this sample is dominated by chlorite (Fe-Mg-rich) with lesser white mica (phengitic; Appendix A). TIR data shows predominantly quartz and albite (Appendix A).

Sample 3779551, a phyllite, is part of a multiply deformed a high-strain zone within the Woolshed Flat Shale in Torren Gorge,

130 14 km east-north-east of Adelaide. Two samples were analysed by the $^{40}Ar/^{39}Ar$ method from this locality. In the nearby Black Hill Conservation Park, a similar phyllite lies in the hanging wall of an east-dipping thrust that places Woolshed Flat Shale over the stratigraphically younger Stonyfell Quartzite. The latter phyllite has a down-dip mineral lineation and a mm-scale crenulation that trends towards ~340° (Fig. 4c). Within this thrust, the phyllite locally contains rafts of dismembered quartzite, which may represent either tectonic slices of Stonyfell Quartzite or sandy interlayers within the Woolshed Flat Shale protolith.

135 Locally, the shear foliation is refolded with secondary open to tight folds, many of which have an axial-planar, spaced

crenulation cleavage (Fig. 4d). Mineralogically the samples comprise phengite and chlorite (Fe-Mg-rich), as well as biotite, carbonates, quartz and albite (Appendix A).

Sample 3779554 is a grey metasiltstone, typical of well laminated siltstones of the Tapley Hill Formation (depositional age
140 643.0 ± 2.4 Ma, Re-Os; Kendall et al., 2006), and possessing an upright, slaty cleavage (Fig. 4e). SWIR analysis suggests that the rock comprises phengitic white mica, while the TIR analysis confirms the presence of quartz, microcline, albite, muscovite and carbonate with minor biotite and phengite (Appendix A).

Sample 3779555, from the early Cambrian Heatherdale Shale at the top of the Normanville Group at Sellick Hill, is the
145 youngest sample in this study. This locality also lies within the chlorite-grade metamorphic zone (Fig. 2). The sample is a fine-grained siltstone that is moderately fractured, being in the hanging wall of the Willunga Fault (Fig. 3), but does not split readily on its slaty cleavage (Fig. 4f). SWIR analysis suggests sample 3779555 comprises phengite and kaolinite, while TIR analysis also shows quartz, microcline, muscovite and albite are present (Appendix A). Note that our sample 3779555 was taken very near to a thin layer of ashfall tuff that has been dated at 514.98 ± 0.22 Ma (zircon U-Pb, chemical abrasion-thermal ionisation
150 mass spectrometry; Betts et al., 2018).

Table 1. Sample details.

Sample	Rock type	Stratigraphic unit	Depositional age	Location	Easting	Northing	Zone (GDA94)
3779555	siltstone	Heatherdale Shale, Normanville Group	515 Ma	Sellick Hill	269649	6086543	54
3779554	siltstone	Tapley Hill Formation, Umberatana Group	643.0 ± 2.4 Ma	Tapley Hill	277441	6120235	54
3779551	phyllite	Woolshed Flat Shale, Burra Group	700-800 Ma	Torrens Gorge	292907	6140205	54
3779552	phyllite	Woolshed Flat Shale, Burra Group	700-800 Ma	Deadmans Pass	294054	6167780	54
3779553	phyllite	Burra Group	700-800 Ma	The Rocks	271453	6216509	54

155
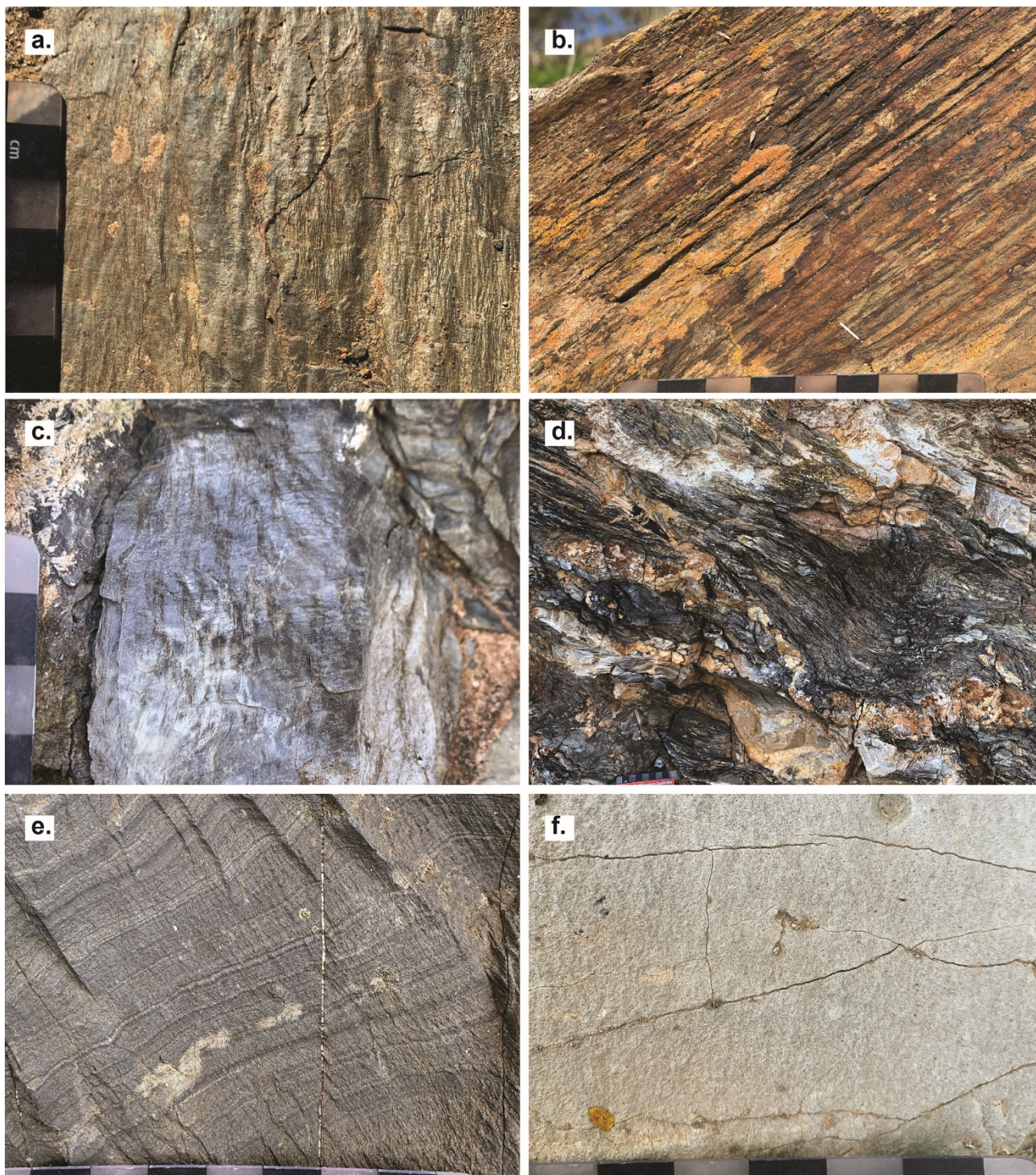
Figure 4: Field photographs of analysed samples. a. Surface of shear fabric in phyllite from the locality of sample 3779553. b. Cross-section view of phyllite at the location of sample 3779552. View towards the south, with moderate east-dipping deformation fabric.
160 **Note orange material is lichen. c. Surface of shear fabric from locality of sample 3779551. d. Cross section view of phyllite in vicinity**

of sample 3779551. This field of view shows rafts of quartzite within the phyllite and complex buckling of the phyllitic-foliation, in places with a new shear fabric developed associated with these structures. e. Detail of laminated metasiltstone of sample 3779554, showing high angle slaty cleavage developed and dipping steeply to the south-east (field of view looking towards north). f. Poorly laminated sediment of the Heatherdale Shale from locality of sample 3779555.

165

4 ^{40}Ar/^{39}Ar analytical methods

As micas in these samples are very fine grained, a whole rock approach was taken to mineral separation. In all cases except 3779551a and b, the separates were wholerock, including inseparable aggregates of micas. In 3779551a and b the aggregates
170 of white mica were more prominent and were therefore separated and analysed. Regions of the rock samples that were the focus of the geochronology were cut from the rock, for example areas where specific fabrics or minerals were located. Only the most pristine material was used from these selected areas. The cut out material was then crushed and sieved to a 420-250μm size fraction. Hand picking was done to select the most suitable material/grains, these were washed in de-ionised water until they were clean. Necessary weights were calculated and the weighed sample grains were packed into aluminium foils
175 and subjected to neutron irradiation at UC Davies nuclear reactor, USA for 12 hours and 5 minutes along with flux monitors, K_2SO_4 and CaF_2 salts for calculation of J-factors, monitoring corrections factors including ^{40}Ar production from potassium. Biotite standard GA-1550 (99.769 ± 0.108 Ma; Renne et al., 2010) was used as the flux monitor. Furnace step-heating diffusion experiments were undertaken at the ^{40}Ar/^{39}Ar Laboratory, Research School of Earth Sciences, Australian National University, Canberra. Complete analytical details are given in Appendix B.

180

Analyses were conducted using a furnace step-heating procedure through an ultrahigh-vacuum extraction line to a *Thermo Fisher* ARGUS-VI multi-collector mass spectrometer. Step-heating diffusion experiments on individual samples were carried out with a temperature-controlled furnace that allows precise control of temperature during step-heating analysis, with heating schedules between 450°C and 1450 °C. GA-1550 standards, were analysed using a CO_2 laser and a linear best fit was then
185 used for the calculation of the J-factor and J-factor uncertainty. Data were reduced using *Noble* 2020 software using the correction factors and J-factors (Appendix B). Stated precisions for ^{40}Ar/^{39}Ar ages include all uncertainties in the measurement of isotope ratios and are quoted at the one sigma level and exclude errors in the age of the flux monitor GA-1550. Reported data have been corrected for system backgrounds, mass discrimination, fluence gradients and atmospheric contamination. ^{40}K abundances and decay constants used are recommended values (Renne et al., 2010). Result tables for each step heating
190 experiment are given in Reid and Forster (2021), with a summary of these ages and their interpretations presented in Table 2.

5 ^{40}Ar/^{39}Ar results

The age spectrum for sample 3779553 yields apparent ages that step progressively upwards over the first 18% gas released to a relatively flat portion of the spectrum to ~75% gas released (Fig. 5a). This flat portion yields an average age of 464.6 ± 4.5

195   Ma. The age spectra steps upwards from c. 464 Ma to a maximum of 549.5 ± 3.7 Ma, at step 21. The final portion of the age spectrum decreases in age to c. 464 Ma, before rising again to a maximum of 705 Ma. The York plot reveals the first 8 steps form a line of progressively decreasing ^{36}Ar/^{40}Ar ratio that represent a less retentive domain (Fig. 5b). The final steps of the experiment yield progressively increasing ^{36}Ar/^{40}Ar ratio, corresponding to higher retentive domain within the crystals.

200   Sample 3779552 has some of the youngest age data from the samples in this study. The first 10% of gas released has ages at 245.9 ±1.8 Ma (Fig. 5c). The ages rise from this minimum to an intermediate asymptote of 371.1 ± 7.8 Ma, while the upper age limit of 480.8 ±2.7 Ma occurs at around 80% gas release. The York plot shows that the early ages to have an atmospheric component, however, most of the heating steps have no or very minor atmospheric component with many steps represent mixing (Fig. 5d).

205

Two different separates of white mica were analysed from sample 3779551, denoted 3779551a and 3779551b. Sample 3779551a comprises silvery-coloured mica intergrown with shiny quartz grains, whereas the mica in sample 3779551b is greenish coloured. Sample 3779551a has an age of 473.1 ± 2.7 Ma that encompasses ~34% gas release, before stepping up to a much older maximum age of 1178.4 ± 5.4 Ma (Fig. 5e). ^{36}Ar/^{40}Ar values have no atmospheric component, with exception of

210   low volume steps at the initial and final portions of the step heating experiment (Fig. 5f). A similar pattern is found in sample 3779551b, which yields an age of 461.5 ± 3.9 Ma over ~54 % gas release, after which the spectrum steps upwards to a maximum age of 1007.8 ± 1.9 Ma (Fig. 5g). The York plot for sample 3779551b has two domains, with the majority with no atmospheric component and mixing in the beginning and final steps (Fig. 5h).

215   The age spectrum for sample 3779554 has apparent ages between c. 386 Ma and 426.9 Ma in the first 15% of ^{39}Ar release (Fig. 5i). At step 9 the age jumps to 511.3 ± 2.8 Ma and then rises consistently to a maximum of 709.6 ± 3.7 Ma at step 20. This staircase spectrum encompasses around 76% of gas released from the sample. After step 20, the age decreases to around c. <516 Ma. The York plot for sample 3779554 steps 1-8 define a population trending towards air composition, however, most steps have low to no to low atmospheric component (Fig. 5j).

220

Sample 3779555 yielded a lower age limit of 435.9 ± 0.4 Ma, rising to an intermediate age population of 532.9 ± 3.3 Ma (~45% ^{39}Ar released; Fig. 5k). The upper limit for this sample is an age of 564.2 ± 7.1 Ma. The York plot shows a small younger age cluster and the main cluster of steps with no atmospheric component, with mixing occurring between these to asymptotes/limits (Fig. 5l).
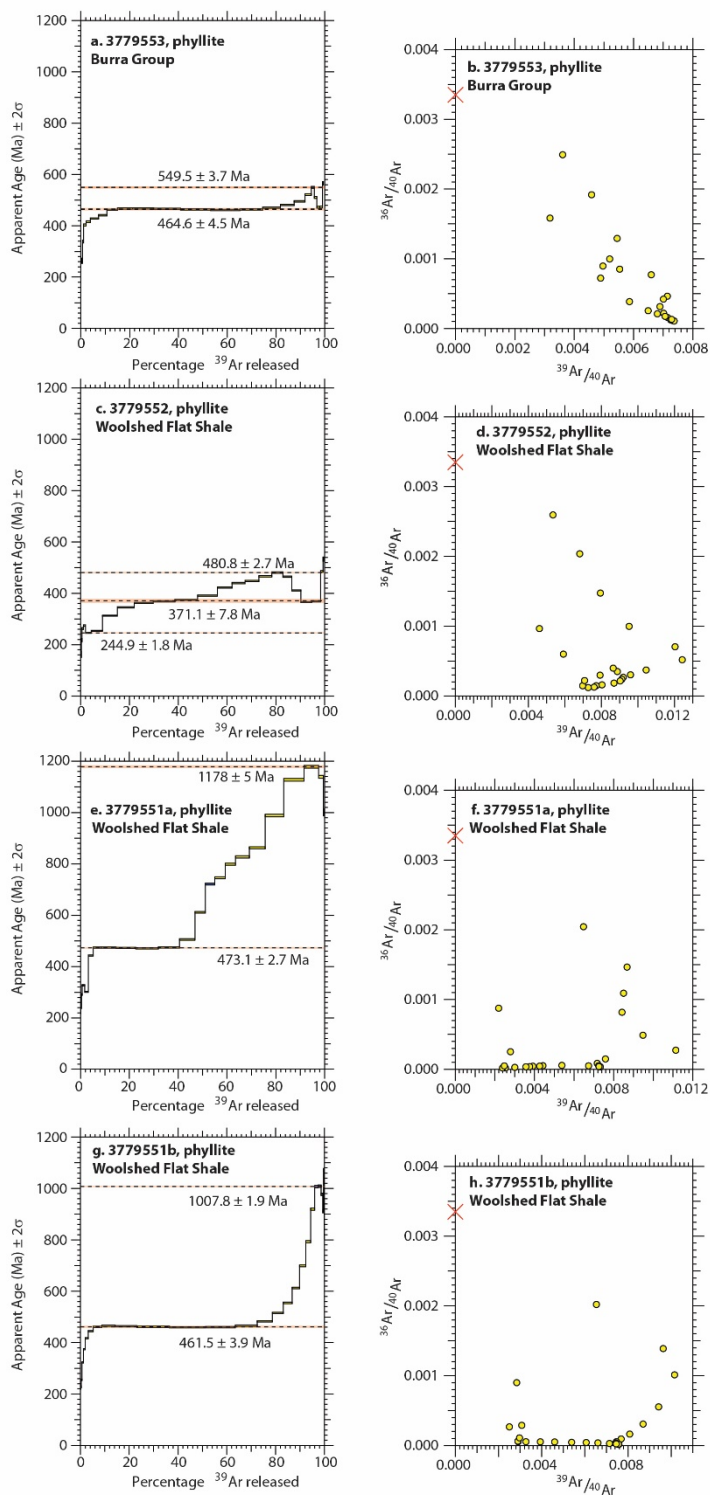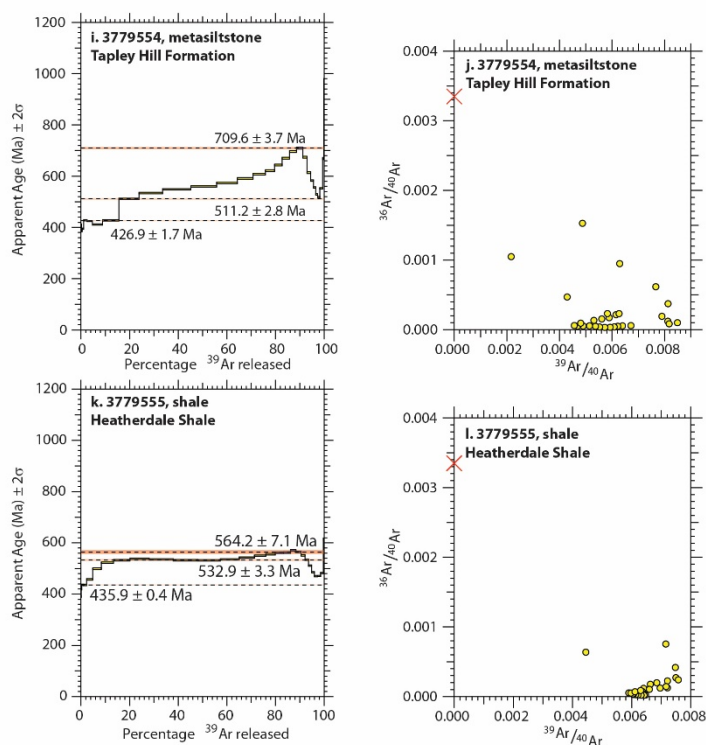
Figure 5: Apparent age spectra and corresponding York plots for samples analysed in this study. Note that all data tables are provided in Reid and Forster (2021) a. Sample 3779553 age spectrum. b. Sample 3779553 York plot. c. Sample 3779552 age spectrum. d. Sample 3779552 York plot. e. Sample 3779551a age spectrum. f. Sample 3779551a York plot. g. Sample 3779551b age spectrum.
230 **h. Sample 3779551b York plot. i. Sample 3779554 age spectrum. j. Sample 3779554 York plot. k. Sample 3779555 age spectrum. l. Sample 3779555 York plot.**

Table 2. Summary of ⁴⁰Ar/³⁹Ar geochronology results.

Sample	Rock type	Stratigraphic unit	Minimum age Ma	Interpretation	Intermediate age Ma	Interpretation	Maximum age Ma	Interpretation
3779555	siltstone	Heatherdale Shale	435.9 ± 0.4	? Deformation	532.9 ± 3.3	Detrital	564.2 ± 7.1	Detrital
3779554	siltstone	Tapley Hill Formation	426.9 ± 2	? Deformation	511.3 ± 2.8	Metamorphism	709.6 ± 3.7	Detrital
3779551a	phyllite	Woolshed Flat Shale	473.1 ± 2.7	Deformation			1178.4 ± 5.4	Detrital
3779551b	phyllite	Woolshed Flat Shale	461.5 ± 3.9	Deformation			1007.8 ± 1.9	Detrital Post-metamorphic cooling?
3779552	phyllite	Woolshed Flat Shale	245.9 ±1.8	uncertain	371.1 ± 7.8	uncertain	480.8 ±2.7	
3779553	phyllite	Burra Group	465 ± 5	Deformation	549.5 ± 3.7	Partly reset detrital age		

235

6 Discussion

6.1 Complex ^{40}Ar/^{39}Ar age spectra and York plots

Single crystal or single mineral ^{40}Ar/^{39}Ar analysis on these samples is not possible due to the fine-grained nature of these low-grade tectono-metamorphic rocks. As a consequence, complex ^{40}Ar/^{39}Ar age spectra are the mostly likely result. Complex

240   ^{40}Ar/^{39}Ar age spectra can result from mixing of multiple age components within a whole rock sample caused by the mixing of different mineralogy (e.g. Kula et al., 2010; Clauer, 2013) or, in the case of single minerals or grains, as a result of different gas domains having a range of diffusion properties (e.g. Lovera et al., 1989; Muston et al., 2021). As discussed by Forster and Lister (2004), the upper asymptote of a staircase age spectrum is the minimum age for crystallisation of the sample and conversely, the lower asymptote is a maximum age for either a less retentive domain within the sample, or a geological resetting

245   event (Fig. 6a). Often complex age spectra result from incomplete degassing of argon during one or more geological events, such as a thermal pulse or deformation event (Fig. 6b; e.g. Wijbrans and Mcdougall, 1988; Baldwin and Lister, 1998; Heizler et al., 1997). Similar staircase age profiles with upper and lower asymptotes have also been measured by whole rock analyses of phyllite from the Caledonian Orogen, Norway (Fig. 6c; Dallmeyer et al., 1988). In the latter example, age gradients were interpreted to reflect incomplete resetting of fine grained white mica during a Caledonian thermal event linked to emplacement

250   of fold nappes onto the Baltic Shield (Dallmeyer et al., 1988).

York plots, or inverse isochron plots, provide an insight into the isotopic composition of the argon released during step heating (Mcdougall and Harrison, 1999). An example of white mica from the South Cyclades Shear Zone, Ios, shows the initial heating steps having a distinct isotopic composition, representing a mixing between atmospheric and the main mineral gas reservoir

255   (Forster and Lister, 2009). This mixing is likely due to the effects of deformation-induced recrystallization (Forster and Lister, 2009). The main gas reservoir is also distinct from the high-temperature heating steps, which yield older apparent ages and represent mixing between atmospheric component and a minor excess ^{40}Ar component.

Complex age spectra and multiple gas domains are present in our samples from the low metamorphic grade rocks in the

260   Delamerian Orogen. The presence of upper age asymptotes that also have distinct isotopic compositions, is consistent with those ages being from distinct gas reservoirs. Taken together, the complex age spectra in this study clearly represent the mixing between older detrital components and younger age components.

265
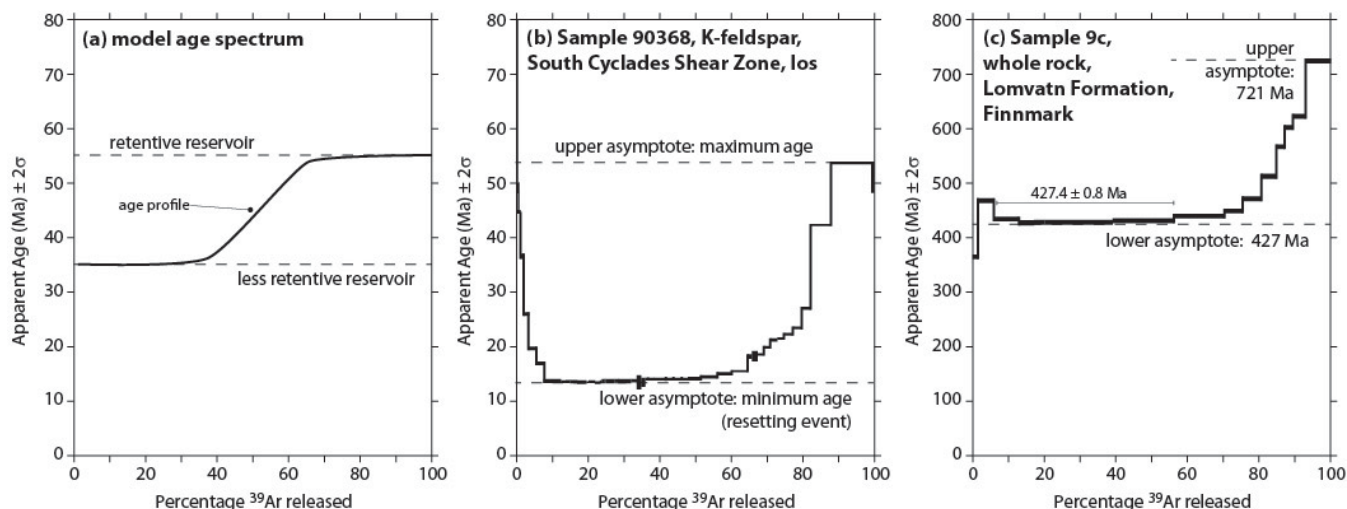
270 **Figure 6. Example complex age spectra. a. Model age spectrum of a simple age spectrum with two component system, mixing between more and less retentive argon gas reservoir. After Forster and Lister (2004). b. Example of K-feldspar with a staircase age spectrum patter resulting from degassing of two diffusion domains, with an upper asymptote defined by the more retentive domain providing a maximum age for the sample, and a lower asymptote representing the minimum age for resetting during greenschist facies metamorphism. Age spectrum and interpretation after Baldwin and Lister (1998). c. Example of complex age spectrum obtained**
275 **from whole rock slate analysis from Dallmeyer et al. (1988). The sample contains both detrital mica and a cleavage with the c. 427 Ma lower asymptote interpreted to reflect timing of cleavage formation and the older ages the influence of detrital mineral with higher argon retentivity (Dallmeyer et al., 1988).**

280 ## 6.2 Detrital ^{40}Ar/^{39}Ar signatures

The transport and deposition of K-bearing minerals can mean the ^{40}Ar/^{39}Ar signature of minerals within sedimentary rocks is representative of events in the source region, rather than indicative of new mineral growth or resetting. This principle has been applied in many settings to reconstruct the early history of orogenic regions now eroded (Stuart, 2002; Blewett et al., 2019), including in the continental foreland basin of the Himalayas (Najman et al., 1997), and the Lachlan Orogen of eastern Australia

285 (Fergusson and Phillips, 2001). As discussed by Fergusson and Phillips (2001) the relative input of different detrital minerals in a whole rock analysis will depend on the abundance, grain size, argon retentivity and respective ages of the different detrital components.

In this study, the age spectra of most samples contain ages older than the age of deposition of the rock. Therefore, these older

290 components must be detrital in origin. Both aliquots of sample of the Woolshed Flat Shale (3779551) yielded the oldest apparently detrital ages, up to 1178 Ma and 1007 Ma. These Mesoproterozoic ages are potentially reflecting input of material derived from the Musgrave Province or equivalent terranes of central Australia, as similar detrital ages are recorded in detrital

zircon U-Pb studies of the Adelaide Superbasin (Lloyd et al., 2020). The oldest components are not the same age in each sample, and this may reflect the different character of the minerals in each. This variation may in turn relate to variation in

295 composition of mica at the scale of individual laminations within the sample. The shape of the age spectra also suggests there is variation between these two sub-samples. In sample 3779551b, the staircase portion of the age pattern begins at ~65 % gas release and is much steeper, compared to 3779551a. This suggests that 3779551b may have undergone a greater degree of recrystallisation at c. 460 Ma and consequently the c. 1007 Ma age represents a minimum detrital component. Increased thermal or microstructural overprinting can have the effect of drawing down the age of pre-existing age components in a sample. The

300 difference in these two age spectra suggests that even small degrees of recrystallisation, such as may occur in small high strain zones at the scale of a single hand sample, can affect the $^{40}Ar/^{39}Ar$ composition of fine-grained rocks.

The remaining samples yield apparent ages closer to their depositional age. Sample 3779554 yields an upper asymptote of 709 Ma. This maximum depositional age of the Tapley Hill Formation, quoted as 654 ± 13 Ma (U-Pb zircon; Lloyd et al., 2020),

305 suggesting the age of the detrital minerals recorded by the $^{40}Ar/^{39}Ar$ data is a minimum of ~50 million years older than the depositional age. This sample is a laminated metasiltstone with a spaced cleavage. The c. 511 Ma age likely approximates the timing of cleavage formation in this rock during the Delamerian Orogeny. The lowest metamorphic grade sample, 3779555 of the Heatherdale Shale, has upper asymptote of 564 Ma, with a younger limit of c. 532 Ma. This shale was deposited at c. 515 Ma (Betts et al., 2018), and consequently, the age spectra suggest that very little of the K-bearing minerals in the shale have

310 been reset either by diagenetic modification, or by tectonothermal processes during the Delamerian Orogeny. The minimal modification to the apparently detrital $^{40}Ar/^{39}Ar$ ages in this sample is consistent with the Heatherdale Shale being the stratigraphically youngest and least metamorphosed rock in this sample set.

A further implication of these detrital mineral ages is to consider the concept that the difference in age between the youngest

315 detritus and deposition of the rock is a response to tectonic setting. Cawood et al. (2012) show that detrital zircon ages in sediment from convergent plate margins are closer in age to the depositional age of the sediment compared to collisional, extensional and intracratonic basins, which contain greater proportions of older ages. On the basis of this relationship outlined by (Cawood et al., 2012) the presence of detrital Mesoproterozoic $^{40}Ar/^{39}Ar$ ages from the Neoproterozoic Woolshed Flat Shale implies that this deposited in an extensional basin, which is the inferred tectonic setting based on stratigraphic and

320 tectonic reconstruction (Preiss, 2000). Conversely, the younger c. 530 Ma component in the Heatherdale Shale, is within ~15 million years of the depositional age of this rock. This age relationship suggests the Cambrian sediments within the Delamerian Orogen formed in a basin setting related to a convergent margin. Indeed, although crustal extension followed immediately after deposition of the Heatherdale Shale with the formation of the Kanmantoo Trough this likely occurred in a back-arc setting, inboard of a newly initiated subduction system along the eastern margin of Gondwana (Foden et al., 2020).

325

6.3 Cooling ages or deformation ages in fine grained samples?

The northern site (sample 3779553) and the Torrens Gorge locality (samples 3779551a and 3779551b) yielded significant portions of the age spectra at c. 460 Ma. In the Delamerian Orogen, syn-tectonic granites were emplaced at c. 514 – 500 Ma and post-tectonic granites at c. 485 Ma (Foden et al., 2006). The c. 460 Ma ages therefore do not lie within the time span of

330 the Delamerian Orogeny as it is understood from the highest metamorphic grade regions of the orogen. This may indicate that the deformation in the thrust sheets that these samples are from continued until, or was active at c. 460 Ma, some 20 million years after the cessation of deformation in the high-metamorphic grade regions of the orogen. Alternatively, it is possible that the fine-grained nature of the samples means that the K-bearing mica in the sample may have remained open to argon diffusion longer than might be expected if the samples were coarser-grained. As a result, the samples may have continued to 'leak' argon

335 until c. 460 Ma when they finally were exhumed to shallow enough crustal levels.

Prolonged cooling through a range of 'closure temperatures' in the detrital minerals and newly grown metamorphic micas may be expected to yield a staircase pattern in the age spectra, as a result of different argon reservoirs cooling as the rock passed through a range of closure temperatures, i.e. a closure temperature window. However, the age spectra for these samples have

340 well-defined plateaus or plateau-like segments at c. 460 Ma, with relatively small portions of the age spectra actually having a staircase pattern. In a study of thrust sheets in the Norwegian Caledonides, progressive changes in age spectra shape from samples in the footwall of a thrust in that study showed decreases in the degree of resetting, which Dallmeyer et al. (1988) interpreted to be a result of recrystallisation during thrusting. The data presented here from the Delamerian Orogen has similar characteristics and could also be interpreted to indicate recrystallisation of mica during thrusting occurred at c. 460 Ma. To

345 further investigate the possibility of c. 460 Ma thrusting in the western Delamerian Orogen, more samples could be taken away from the thrust zones to investigate progressive changes in argon retentivity.

In contrast, sample 3779552 has an upper age limit of 480 Ma and the age spectrum does show a stepwise progression of ages from ages as young as c. 245 Ma, with an intermediate age at c. 371 Ma. These ages are considerably younger than other ages

350 obtained in this study and suggest that this sample has a complex history of mica growth and cooling. One interpretation of the spectrum could be that c. 480 Ma is a minimum age for peak metamorphism and deformation in the sample, recorded only in the higher temperature heating steps. Similar Early Ordovician ages are recorded in biotite from earlier K-Ar dating in the eastern Mt Lofty Ranges (Milnes et al., 1977; Turner et al., 1996). The even younger ages may record partial resetting of low retentivity domains within K-bearing minerals in the sample during the Carboniferous and Permian. Apatite fission track

355 studies in the region also suggest exhumation at this time (Holford et al., 2021), possibly as a result of reactivation of faults across the southern Mt Lofty Ranges (Preiss, 2019). Sample 3779552 is from the hangingwall of the Para Fault, which has a neotectonic expression, and there is evidence that many of the neotectonic faults of the Adelaide region have been reactivated

multiple times, sometimes involving reversal of movement sense (Preiss, 2019). Further dating in this region is required to better understand the context for the results obtained from sample 3779552.

360

In summary, the previous ^{40}Ar/^{39}Ar dating from the higher metamorphic grade regions and magmatic rocks of the Delamerian Orogen have suggested that cooling was relatively rapid, with exhumation of these rocks into the upper crust by c. 480 Ma (Turner et al., 1996). Importantly, these interpretations suggested that uplift of the Delamerian was rapid and connected to mantle upwelling, ie. lithospheric extension, as manifest also in the belt of post-tectonic and A-type granites in the region

365 (Turner et al., 1996; Foden et al., 2020). Our new data on the rocks exposed in the western Mt Lofty Ranges suggest that this region was exhumed later than the higher metamorphic grade rocks in the east. This has implications for our understanding of the tectonic architecture of the Delamerian Orogen. It may suggest that some, if not all, of the major thrust sheets interpreted in the western Mt Lofty Ranges (Fig. 3) were active or, more likely, were re-activated at c. 460 Ma. Tectonic forces that led to these c. 460 Ma events are likely related to far-field drivers along the then active eastern margin of Gondwana, which is

370 now preserved in the Lachlan Orogen (e.g. Moresi et al., 2014).

7 Conclusion

Isotopic analyses of low metamorphic grade rocks can be difficult to interpret as these are a mixture of detrital and newly grown, diagenetic or metamorphic minerals, which are not easy to resolve. In this study, we have applied the ^{40}Ar/^{39}Ar method with careful furnace step heating analysis of whole rock samples of low-grade metamorphic rocks. Key to interpreting the

375 complex ^{40}Ar/^{39}Ar age spectra is the idea that the shape of the spectra themselves is informative as to the nature of the various gas reservoirs in a sample, and asymptotes within the spectra define minimum and maximum ages for these components (Forster and Lister, 2004; Forster and Lister, 2009). Data from this study shows that the Neoproterozoic rocks of the southern Delamerian Orogen preserve detrital mineral components up to 1178 Ma in age, while Cambrian shale yields detrital mineral components with ages of c. 564 and c. 532 Ma and hence much closer to the age of deposition. Applying the concept that

380 younger detrital minerals are found in convergent margin sediment as has been shown from detrital zircon studies (Cawood et al., 2012), the new data from the Delamerian Orogen support the notion that the Cambrian was a time of convergent margin tectonics (i.e. subduction) along the eastern margin of Gondwana (Foden et al., 2020). Application of ^{40}Ar/^{39}Ar dating to low metamorphic grade successions across orogens with poorly defined tectonic settings may therefore be a useful tool to test tectonic settings, with implications for continental reconstruction models.

385

Finally, the younger asymptotes in our data are some 20 million years younger than the timing of the last phases of the Delamerian Orogeny documented from studies of granitic intrusions and amphibolite-grade metamorphic fabrics (Foden et al., 2006; Foden et al., 2020). The two possible interpretations of the younger age components are that they are either (i) a record of regional cooling, with the minerals being passively cooled through their closure temperatures as a result of isotherm

390 relaxation, or (ii) a record of deformation-induced recrystallisation. The second interpretation implies that some zones of phyllite in the Delamerian Orogen could well have formed at, or continued until, sometime after the main phase of deformation recorded in higher metamorphic grade regions of the orogen. Further work is required to test these hypotheses, however, the new data point to the possibility that widespread application of this methodology, likely in combination with other methods such as Rb-Sr dating (e.g. Zack and Hogmalm, 2016), is a pathway forward for analysis of low metamorphic grade rocks as a

395 complement to analysis of metamorphic rocks form higher grade regions within orogens by other isotopic methods (e.g. zircon, monazite U-Pb) and will provide a more holistic understanding of orogenic regions.

Appendix A. Hyperspectral mineralogical methods and results

Hyperspectral mineralogy methods

400 Samples were mineralogically characterised with a Hylogger-3™ (Schodlok et al., 2016), instrument at the Geological Survey of South Australia, Drill Core Reference Library, Adelaide. The HyLogger-3™ collects multiple data types including reflectance from the Visible-Near Infrared, Shortwave Infrared (VNIR-SWIR, 380-2,500 nm) and Thermal Infrared (TIR, 6,500 - 14,000 nm), high-resolution imagery and laser profilometer data at 4 mm resolution. Although this instrument is primarily designed to scan drill core, it is adaptable to collect data from a variety of geological materials. Each rock sample

405 was measured with five passes of the HyLogger™. The resulting spectral data was processed to exclude noisy and unwanted spectra using The Spectral Geologist™ v8.1.0.3 (TSG) software (Mason et al., 2020). Two algorithms, The Spectral Assistant™ (TSA) and joint Constrained Least Squares (jCLST), unmix the of spectral data and produces a semi-quantitative mineralogical result for SWIR and TIR. In this study, spectral results were obtained via traverses across each sample, with an average mineralogical composition compiled from both the SWIR and TIR spectrometers, as each wavelength range is

410 diagnostic for different minerals. Note that different minerals can appear in both SWIR and TIR analysis and that the total mineralogy identified by each spectral range is not necessarily indicative of the entire mineralogy of the sample. These data are used as a guide to the major mineral components, in particular the fine-grained minerals such as mica that are significant for the present [40]Ar/[39]Ar study.

415 Scalars are algorithms applied within TSG designed to interpret diagnostic absorption features related to specific mineral species. A scalar developed by Haest et al. (2012) examines the wavelength change of the 2,200 nm Al-OH absorption feature (Figure A1), known to distinguish endmembers of white mica. Shorter wavelengths are indicative of a muscovitic composition and longer wavelengths demonstrate a phengitic white mica.

420 Hylogger[TM] results for each sample are given in the following and are shown as:

      a) plain light high-resolution image of each sample,

b) the same image with the sample divided into a series of 'runs' in which the main mineralogy identified by SWIR and TIR analysis is shown in coloured bars below the image to demonstrate spatial variability within the sample, with the colour of the bars indicated in the adjacent legend,

425

c) pie diagram compositional summary representing semi-quantitative HyLogger™ data identified in the SWIR wavelength range,

d) pie diagram compositional summary representing semi-quantitative HyLogger™ data identified in the TIR wavelength range.

430
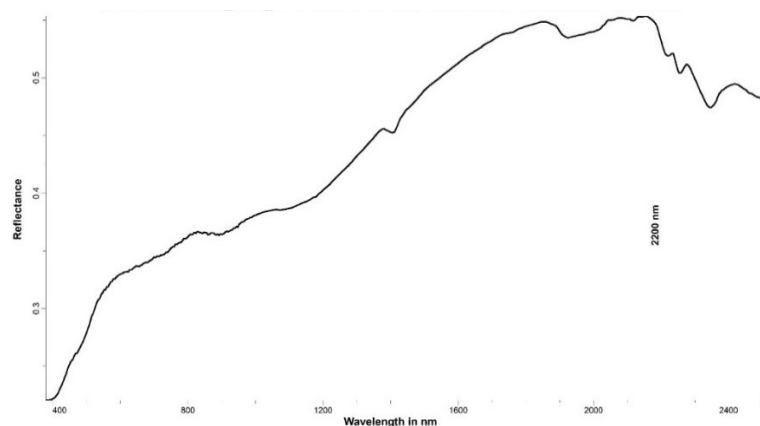
Figure A1. A representative spectral measurement from a sample in this study, the 2,200 nm feature is highlighted to demonstrate its position relative to the VNIR-SWIR spectral signature.

435

Hyperspectral mineralogy results for each sample analysed in this study
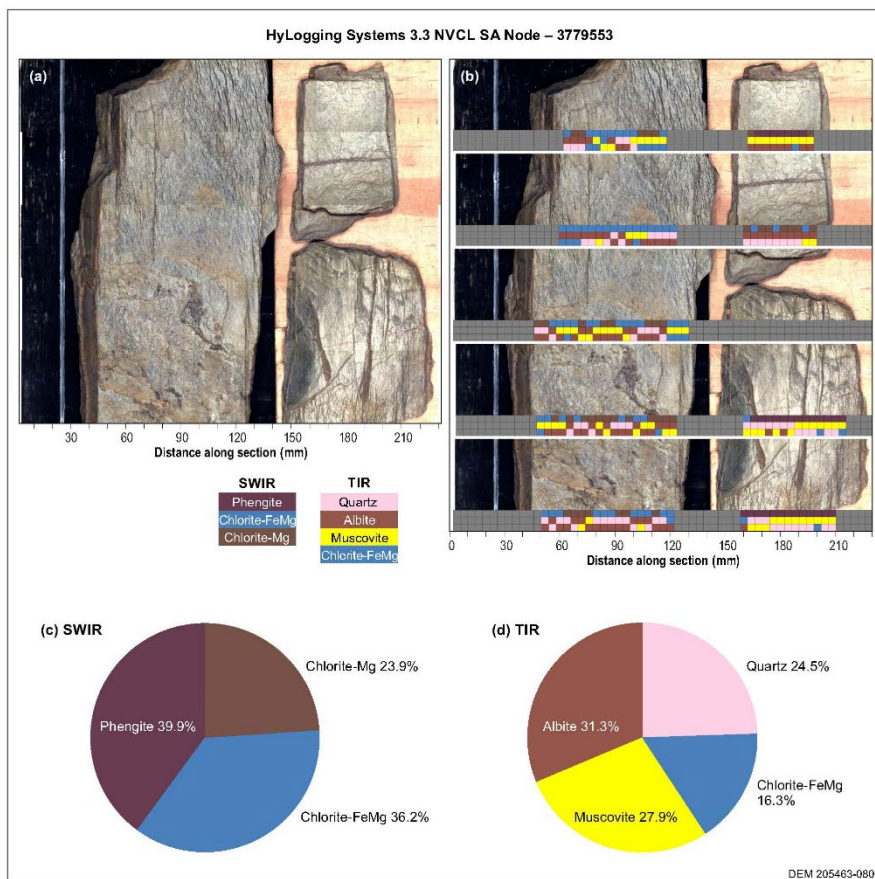
Figure A2. Hyperspectral mineralogy results for sample 3779553.
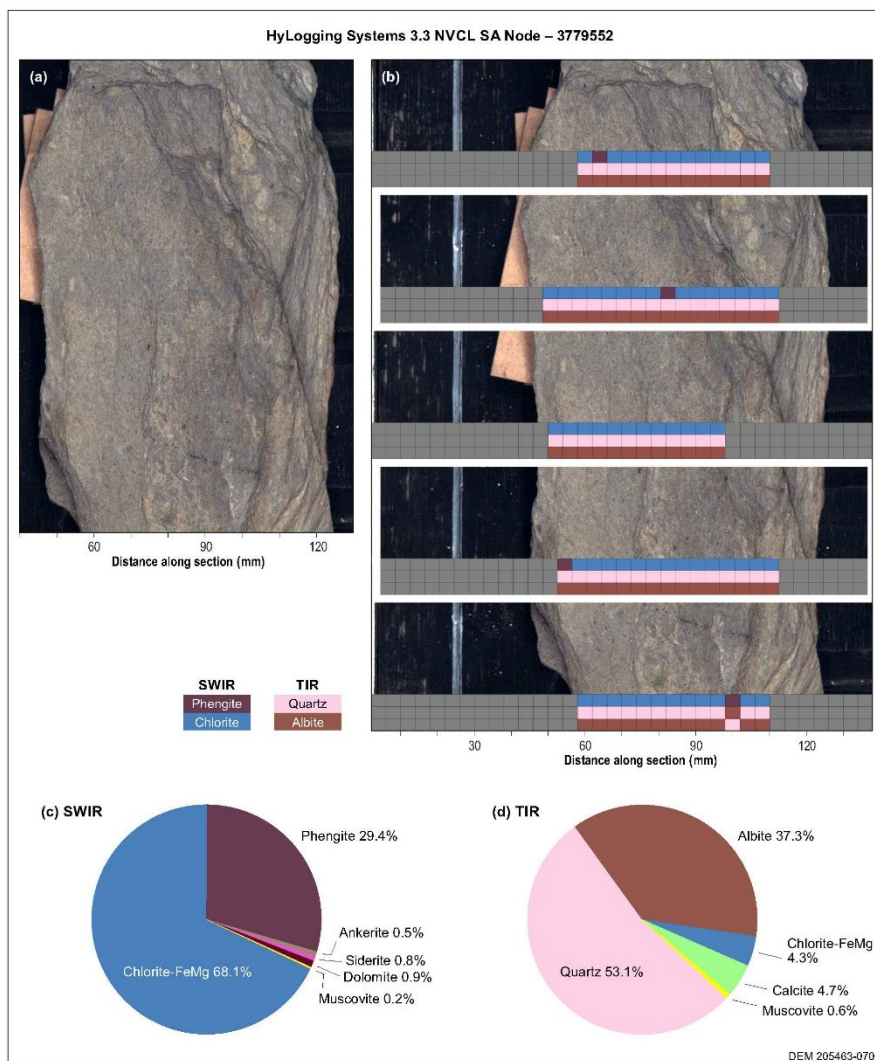
Figure A3. Hyperspectral mineralogy results for sample 3779552.

440
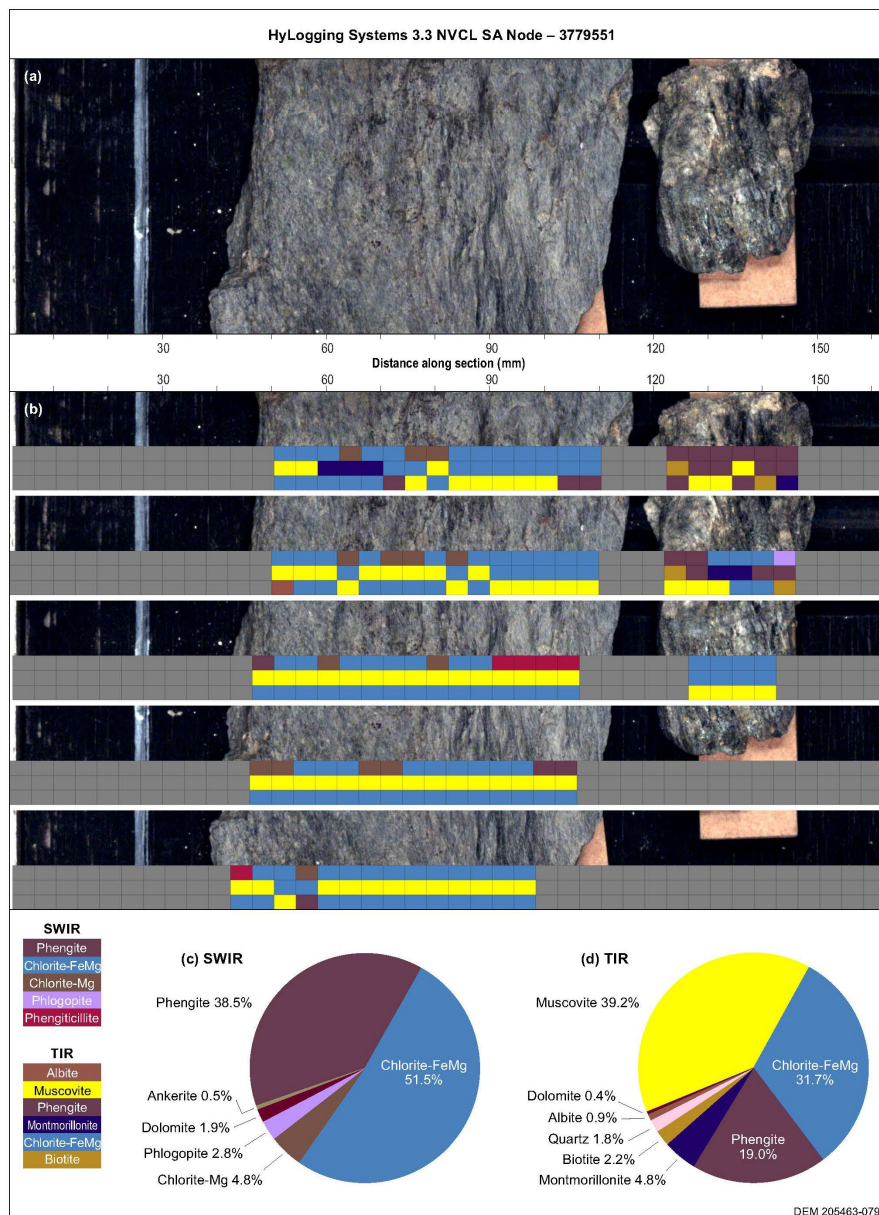
Figure A4. Hyperspectral mineralogy results for sample 3779551.

445

Figure A5. Hyperspectral mineralogy results for sample 3779554.
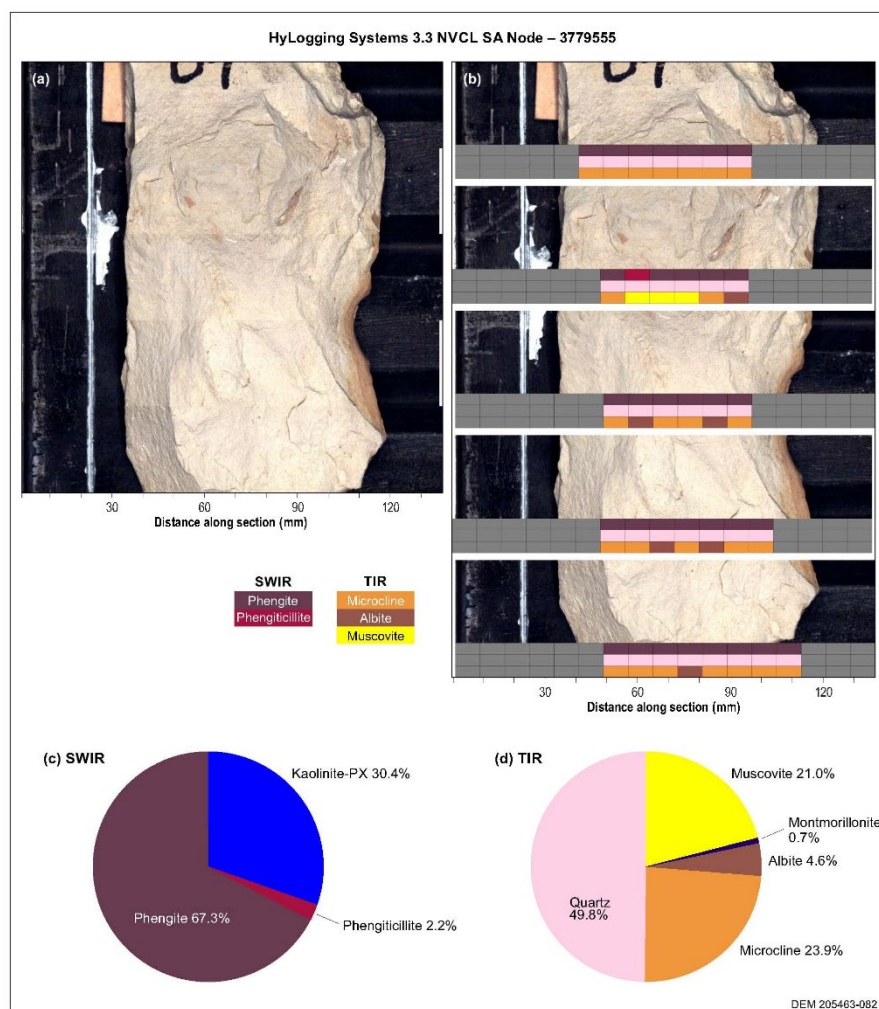
450 **Figure A6. Hyperspectral mineralogy results for sample 3779555.**

References for Appendix A:

455 Haest, M., Cudahy, T., Laukamp, C., and Gregory, S.: Quantitative Mineralogy from Infrared Spectroscopic Data. I. Validation of Mineral Abundance and Composition Scripts at the Rocklea Channel Iron Deposit in Western Australia, Economic Geology, 107, 209-228, 10.2113/econgeo.107.2.209, 2012.

Mason, P., Berman, M., Guo, Y., Warren, P., Lagerstrom, R., Bischof, L., Huntington, J., and Rodger, A.: The Spectral Geologist (8.1.0.3), CSIRO [code], 2020.

460   Schodlok, M. C., Whitbourn, L., Huntington, J., Mason, P., Green, A., Berman, M., Coward, D., Connor, P., Wright, W., Jolivet, M., and Martinez, R.: HyLogger-3, a visible to shortwave and thermal infrared reflectance spectrometer system for drill core logging: functional description, Australian Journal of Earth Sciences, 63, 929-940, 10.1080/08120099.2016.1231133, 2016.

465   **Appendix B. Details of ^{40}Ar/^{39}Ar analytical methods**

Sample irradiation details:

Irradiation of samples for ^{40}Ar/^{39}Ar analysis is required, this was undertaken at the University of California Davis McClellan Nuclear Research Centre, CA, US. The samples in this study were irradiated in ANU CAN #36 and the canister had 1.0mm cadmium shielding (Tetley et al., 1980). For each sample, calculated amounts of grains were weighed, recorded and wrapped

470   in labelled aluminium packets in preparation for irradiation. The sample filled foils were placed into a quartz irradiation canister together with aliquots of the flux monitor GA1550. The GA1550 standards are dispersed throughout the irradiated canister, between the unknown age samples. In addition, packets containing K_2SO_4 and CaF_2 were placed in the middle of the canister to monitor ^{40}Ar production from potassium. Irradiated samples were unwrapped upon their return to the Australian National University, and then rewrapped in tin foil in preparation for analysis in the mass spectrometer.

475

^{40}Ar/^{39}Ar procedures and analysis information:

Samples and standards were analysed in the Argon Laboratory at the Research School of Earth Science, The Australian National University, Canberra, Australia using a *Thermo Fisher* ARGUS-VI multi-collector mass spectrometer. A furnace step-heating technique was used to extract argon isotopes from the samples to ensure 100% release of ^{39}Ar, while the flux

480   monitors crystals (GA1550 biotite) were fused using a CO_2 continuous-wave laser; gases extracted from both the samples and standards were analysed in the Argus VI mass spectrometer. Samples had been wrapped in tin foil so as to melt the tin and pump away the gases prior to the sample analysis. The furnace was degassed 4 times at 1,450°C for 15 minutes and the gas pumped away prior to the loading of the subsequent sample. Gas released from flux monitors and each step of sample analyses was exposed to three different Zr-Al getters to remove active gases for 10 minutes and the purified gas was isotopically

485   analysed in the mass spectrometer. Samples were analysed with 30 steps and with temperatures of the overall schedule rising from 450° to 1,450°C (Reid and Forster, 2021). The ^{40}Ar/^{39}Ar dating technique is adapted from Mcdougall and Harrison (1999) and described in Forster and Lister (2009).

The background levels were measured and subtracted from all analysis, laser and furnace. For example, backgrounds were

490   measured prior to every step of the sample analysis and subtracted from the isotope intensities for ^{40}Ar, ^{39}Ar, ^{38}Ar, ^{37}Ar and ^{36}Ar. The nuclear interfering values for the correction factors for the isotopes are listed below. These are measured for the

reactions and uncertainties of $(^{36}Ar/^{37}Ar)_{Ca}$, $(^{39}Ar/^{37}Ar)_{Ca}$, $(^{40}Ar/^{39}Ar)_K$, $(^{38}Ar/^{39}Ar)_K$ and $(^{38}Ar)_{Cl}/(^{39}Ar)_K$, and were calculated prior to sample analysis.

ANU IRRADIATION CAN #36	
Flux Monitor: GA1550 @ 99.769 ±0.108 Ma (Renne et al 2010)	
$(^{36}Ar/^{37}Ar)_{Ca}$ correction factor	1.012835E-4
$(^{39}Ar/^{37}Ar)_{Ca}$ correction factor	8.469432E-4
$(^{40}Ar/^{39}Ar)_K$ correction factor	1.340092E-1
$^{38}Ar/^{39}Ar)_K$ correction factor	1.054454E-2
$(^{38}Ar)_{Cl}/(^{39}Ar)_K$ correction factor	8.184720E-2
Ca/K conversion factor	1.90
Discrimination factor	1.00441 ± 0.185%
Lambda ^{40}K	5.54920E-10
Total irradiation power	12.08 MW
Irradiation Date	August 11-12, 2020

495

Sample	Field Way Point	Foil	J-Factor	J-Factor uncertainty	Mineral	Measurement Date
3779554	WP 12-01	M03	2.24374E-03	0.2425	Whole Rock	22 Mar,2021
3779555	WP 13-01	M11	2.23290E-03	0.2425	Whole Rock	24 Mar,2021
3779552	WPT 09-01	M17	2.22762E-03	0.2426	Whole Rock	30 Mar,2021
3779553	WPT 10	M21	2.22250E-03	0.2426	White Mica	12-Mar-2021
3779551a	WPT 5-01	M27	2.21396E-03	0.2427	Whole Rock	05 Apr,2021
3779551b	WPT 5-02	M28	2.21225E-03	0.2427	Whole Rock	06 Apr,2021

^{40}K abundances and decay constants are calculated per Renne et al. (2010). Stated precisions for $^{40}Ar/^{39}Ar$ ages include all uncertainties in the measurement of isotope ratios and are quoted at the one sigma level and exclude errors in the age of the

500   fluence monitor GA1550 (99.769 ±0.108 Ma). The reported data have been corrected for system backgrounds, mass discrimination, fluence gradients and atmospheric contamination. GA1550 standards were analysed and a linear best fit was then used for the calculation of the J-factor and J-factor uncertainty.

Data reductions were done with an adapted version of *Noble* Software (2020, written and adapted by the Australian National

505   University Argon Laboratory). The data reduction was based on optimising MSWD (the mean square of weighted deviates) of isotopes intensities with an exponential best fit methodology. The discrimination factor was calculated by analysing five Air

Shots analysis on either side of sample analysis, based on the atmospheric $^{40}Ar/^{36}Ar$ ratio (298.57; see Lee et al., 2006), and the calculation of the 1amu was used for the discrimination factor.

510    $^{40}Ar/^{39}Ar$ isotopic data of the sample is supplied in the Reid and Forster (2021), which includes details on: the heating schedule, Argon isotopes abundances and uncertainty levels, %Ar*, $^{40}Ar*/^{39}Ar(K)$, Cumulative ^{39}Ar%, Age and uncertainty, Ca/K, Cl/K, J-factor and J-factor uncertainty, noting that the fractional uncertainties are shown as %, and are stated in the headings of the appropriate columns. Uncertainty levels of the calculated ages are at one sigma.

515

Author contributions

Study design and field work by AR, MF, WP, SC. Sample preparation and analyses by MF, NG, AC. Interpretation and data analysis by all. AR prepared the manuscript with contributions from all co-authors.

Competing interests

520   The authors declare that they have no conflict of interest.

Acknowledgements

This work has been supported by the Mineral Exploration Cooperative Research Centre whose activities are funded by the Australian Government's Cooperative Research Centre Program. This is MinEx CRC Document 20**/***. The work is also supported by the Geological Survey of South Australia. Georgina Gordon is thanked for assistance with Hylogger^{TM} analysis
525   at the Department for Energy and Mining's South Australian Drill Core Reference Library, Adelaide.

References

Baldwin, S. L. and Lister, G. S.: Thermochronology of the South Cyclades Shear Zone, Ios, Greece: Effects of ductile shear
530   in the argon partial retention zone, Journal of Geophysical Research: Solid Earth, 103, 7315-7336,
https://doi.org/10.1029/97JB03106, 1998.

Betts, M. J., Paterson, J. R., Jacquet, S. M., Andrew, A. S., Hall, P. A., Jago, J. B., Jagodzinski, E. A., Preiss, W. V., Crowley,
J. L., Brougham, T., Mathewson, C. P., García-Bellido, D. C., Topper, T. P., Skovsted, C. B., and Brock, G. A.: Early Cambrian

chronostratigraphy and geochronology of South Australia, Earth-Science Reviews, 185, 498-543,
535 https://doi.org/10.1016/j.earscirev.2018.06.005, 2018.

Blewett, S. C. J., Phillips, D., and Matchan, E. L.: Provenance of Cape Supergroup sediments and timing of Cape Fold Belt
orogenesis: Constraints from high-precision 40Ar/39Ar dating of muscovite, Gondwana Research, 70, 201-221,
https://doi.org/10.1016/j.gr.2019.01.009, 2019.

Burtt, A. C. and Phillips, D.: 40Ar/39Ar dating of muscovite from a pegmatite in Kinchina Quarry, near Murray Bridge, MESA
540 Journal, 28, 50-52, 2003.

Cawood, P. A.: Terra Australis Orogen: Rodinia breakup and development of the Pacific and Iapetus margins of Gondwana
during the Neoproterozoic and Paleozoic, Earth-Science Reviews, 69, 249-279,
https://doi.org/10.1016/j.earscirev.2004.09.001, 2005.

Cawood, P. A., Hawkesworth, C. J., and Dhuime, B.: Detrital zircon record and tectonic setting, Geology, 40, 875-878,
545 10.1130/g32945.1, 2012.

Cawood, P. A., Johnson, M. R. W., and Nemchin, A. A.: Early Palaeozoic orogenesis along the Indian margin of Gondwana:
Tectonic response to Gondwana assembly, Earth and Planetary Science Letters, 255, 70-84,
https://doi.org/10.1016/j.epsl.2006.12.006, 2007.

Chan, Y.-C., Crespi, J. M., and Hodges, K. V.: Dating cleavage formation in slates and phyllites with the 40Ar/39Ar laser
550 microprobe: an example from the western New England Appalachians, USA, Terra Nova, 12, 264-271,
https://doi.org/10.1046/j.1365-3121.2000.00308.x, 2000.

Clauer, N.: The K-Ar and 40Ar/39Ar methods revisited for dating fine-grained K-bearing clay minerals, Chemical Geology,
354, 163-185, 10.1016/j.chemgeo.2013.05.030, 2013.

Cosca, M. A., Hunziker, J. C., Huon, S., and Masson, H.: Radiometric age constraints on mineral growth, metamorphism, and
555 tectonism of the Gummfluh Klippe, Briançonnais domain of the Préalpes, Switzerland, Contributions to Mineralogy and
Petrology, 112, 439-449, 10.1007/BF00310776, 1992.

Dallmeyer, R. D. and Takasu, A.: 40Ar/39Ar ages of detrital muscovite and whole-rock slate/phyllite, Narragansett Basin, RI-
MA, USA: implications for rejuvenation during very low-grade metamorphism, Contributions to Mineralogy and Petrology,
110, 515-527, 10.1007/BF00344085, 1992.

560 Dallmeyer, R. D., Mitchell, J. G., Pharaoh, T. C., Reuter, A., and Andresen, A.: K-Ar and 40Ar/39Ar whole-rock ages of
slate/phyllite from allochthonous basement and cover in the tectonic windows of Finnmark, Norway: Evaluating the extent
and timing of Caledonian tectonothermal activity, GSA Bulletin, 100, 1493-1501, 10.1130/0016-
7606(1988)100<1493:Kaaaaw>2.3.Co;2, 1988.

Dunlap, W. J., Teyssier, C., McDougall, I., and Baldwin, S.: Ages of deformation from K/Ar and 40Ar/39Ar dating of white
565 micas, Geology, 19, 1213-1216, 10.1130/0091-7613(1991)019<1213:Aodfka>2.3.Co;2, 1991.

Dymoke, P. and Sandiford, M.: Phase relationships in Buchan facies series pelitic assemblages: calculations with application
to andalusite-staurolite parageneses in the Mount Lofty Ranges, South Australia, Contributions to Mineralogy and Petrology,
110, 121-132, 10.1007/BF00310886, 1992.

Fergusson, C. L. and Phillips, D.: 40Ar/39Ar and K–Ar age constraints on the timing of regional deformation, south coast of New South Wales, Lachlan Fold Belt: Problems and implications, Australian Journal of Earth Sciences, 48, 395-408, 10.1046/j.1440-0952.2001.00866.x, 2001.

Flottmann, T. and James, P.: Influence of basin architecture on the style of inversion and fold-thrust belt tectonics—the southern Adelaide Fold-Thrust Belt, South Australia, Journal of Structural Geology, 19, 1093-1110, https://doi.org/10.1016/S0191-8141(97)00033-3, 1997.

Flottmann, T., Haines, P., Jago, J., James, P., Belperio, A. P., and Gum, J.: Formation and reactivation of the Cambrian Kanmantoo Trough, SE Australia: implications for early Palaeozoic tectonics at eastern Gondwana's plate margin Journal of the Geological Society, 155, 525-539, 1998.

Foden, J., Elburg, M. A., Dougherty-Page, J., and Burtt, A.: The Timing and Duration of the Delamerian Orogeny: Correlation with the Ross Orogen and Implications for Gondwana Assembly, The Journal of Geology, 114, 189-210, 2006.

Foden, J., Sandiford, M., Dougherty-Page, J., and Williams, I.: Geochemistry and geochronology of the Rathjen Gneiss: Implications for the early tectonic evolution of the Delamerian Orogen, Australian Journal of Earth Sciences, 46, 377-389, 10.1046/j.1440-0952.1999.00712.x, 1999.

Foden, J., Elburg, M., Turner, S., Clark, C., Blades, M. L., Cox, G., Collins, A. S., Wolff, K., and George, C.: Cambro-Ordovician magmatism in the Delamerian orogeny: Implications for tectonic development of the southern Gondwanan margin, Gondwana Research, 81, 490-521, https://doi.org/10.1016/j.gr.2019.12.006, 2020.

Forster, M. and Lister, G.: Core-complex-related extension of the Aegean lithosphere initiated at the Eocene-Oligocene transition, Journal of Geophysical Research: Solid Earth, 114, https://doi.org/10.1029/2007JB005382, 2009.

Forster, M. A. and Lister, G. S.: The interpretation of 40Ar/39Ar apparent age spectra produced by mixing: application of the method of asymptotes and limits, Journal of Structural Geology, 26, 287-305, https://doi.org/10.1016/j.jsg.2003.10.004, 2004.

Glen, R. A. and Cooper, R. A.: Evolution of the East Gondwana convergent margin in Antarctica, southern Australia and New Zealand from the Neoproterozoic to latest Devonian, Earth-Science Reviews, 220, 103687, https://doi.org/10.1016/j.earscirev.2021.103687, 2021.

Heizler, M. T., Ralser, S., and Karlstrom, K. E.: Late Proterozoic (Grenville?) deformation in central New Mexico determined from single-crystal muscovite 40Ar/39Ar age spectra, Precambrian Research, 84, 1-15, https://doi.org/10.1016/S0301-9268(96)00053-8, 1997.

Holford, S. P., Green, P. F., Duddy, I. R., Hillis, R. R., Hill, S. M., and Stoker, M. S.: Preservation of late Palaeozoic glacial rock surfaces by burial prior to Cenozoic exhumation, Fleurieu Peninsula, southeastern Australia, Journal of the Geological Society, 10.1144/jgs2020-250, 2021.

Kendall, B., Creaser, R. A., and Selby, D.: Re-Os geochronology of postglacial black shales in Australia: Constraints on the timing of "Sturtian" glaciation, Geology, 34, 729-732, 10.1130/g22775.1, 2006.

Kirkland, C. L., Daly, J. S., Chew, D. M., and Page, L. M.: The Finnmarkian Orogeny revisited: An isotopic investigation in eastern Finnmark, Arctic Norway, Tectonophysics, 460, 158-177, https://doi.org/10.1016/j.tecto.2008.08.001, 2008.

Kirschner, D. L., Masson, H., and Cosca, M. A.: An 40Ar/39Ar, Rb/Sr, and stable isotope study of micas in low-grade fold-and-thrust belt: an example from the Swiss Helvetic Alps, Contributions to Mineralogy and Petrology, 145, 460-480,
605   10.1007/s00410-003-0461-2, 2003.

Kula, J., Spell, T. L., and Zanetti, K. A.: 40Ar/39Ar analyses of artificially mixed micas and the treatment of complex age spectra from samples with multiple mica populations, Chemical Geology, 275, 67-77, https://doi.org/10.1016/j.chemgeo.2010.04.015, 2010.

Lee, J.-Y., Marti, K., Severinghaus, J. P., Kawamura, K., Yoo, H.-S., Lee, J. B., and Kim, J. S.: A redetermination of the
610   isotopic abundances of atmospheric Ar, Geochimica et Cosmochimica Acta, 70, 4507-4512, https://doi.org/10.1016/j.gca.2006.06.1563, 2006.

Lloyd, J. C., Blades, M. L., Counts, J. W., Collins, A. S., Amos, K. J., Wade, B. P., Hall, J. W., Hore, S., Ball, A. L., Shahin, S., and Drabsch, M.: Neoproterozoic geochronology and provenance of the Adelaide Superbasin, Precambrian Research, 350, 105849, https://doi.org/10.1016/j.precamres.2020.105849, 2020.

615   Lovera, O. M., Richter, F. M., and Harrison, T. M.: The ^{40}Ar/^{39}Ar thermochonometry for slowly cooled samples having a distribution of diffusion domain sizes, Journal of Geophysical Research, 94, 17,917-917,935, 1989.

Mancktelow, N. S.: The structure of the southern Adelaide Fold Belt, South Australia, in: The evolution of a late Precambrian-early Paleozoic rift complex: the Adelaide Geosyncline, edited by: Jago, J. B., and Moore, P. S., Geological Society of Australia Special Publication 16, 369–395, 1990.

620   McDougall, I. and Harrison, T. M.: Geochronology and thermochronology by the ^{40}Ar/^{39}Ar method, 2nd, Oxford University Press, New York, 212 pp.1999.

Milnes, A. R., Compston, W., and Daily, B.: Pre- to syn-tectonic emplacement of early Palaeozoic granites in southeastern South Australia, Journal of the Geological Society of Australia, 24, 87-106, 10.1080/00167617708728969, 1977.

Moresi, L., Betts, P. G., Miller, M. S., and Cayley, R. A.: Dynamics of continental accretion, Nature, 508, 245-248,
625   10.1038/nature13033 http://www.nature.com/nature/journal/v508/n7495/abs/nature13033.html#supplementary-information, 2014.

Muston, J., Forster, M., Vasegh, D., Alderton, C., Crispin, S., and Lister, G.: Direct dating of overprinting fluid systems in the Martabe epithermal gold deposit using highly retentive alunite, Geochronology Discuss., 2021, 1-31, 10.5194/gchron-2021-25, 2021.

630   Najman, Y. M. R., Pringle, M. S., Johnson, M. R. W., Robertson, A. H. F., and Wijbrans, J. R.: Laser 40Ar/39Ar dating of single detrital muscovite grains from early foreland-basin sedimentary deposits in India: Implications for early Himalayan evolution, Geology, 25, 535-538, 10.1130/0091-7613(1997)025<0535:Laados>2.3.Co;2, 1997.

Offler, R. and Fleming, P. D.: A synthesis of folding and metamorphism in the Mt Lofty Ranges, South Australia, Journal of the Geological Society of Australia, 15, 245-266, 10.1080/00167616808728697, 1968.

635   Phillips, D., Fu, B., Wilson, C. J. L., Kendrick, M. A., Fairmaid, A. M., and Miller, J. M.: Timing of gold mineralisation in the western Lachlan Orogen, SE Australia: A critical overview, Australian Journal of Earth Sciences, 59, 495-525, 10.1080/08120099.2012.682738, 2012.

Preiss, W. V.: The Adelaide Geosyncline: Late Proterozoic stratigraphy, sedimentation, palaeontology and tectonics, Geological Survey of South Australia - Bulletin 53, Adelaide, 428 pp.1987.

640 Preiss, W. V.: Delamerian Orogeny, in: The geology of South Australia; Volume 2, The Phanerozoic, edited by: Drexel, J. F., Preiss, W. V., and Parker, A. J., Geological Survey of South Australia - Bulletin 54 Adelaide, 45-59, 1995.

Preiss, W. V.: The Adelaide Geosyncline of South Australia and its significance in Neoproterozoic continental reconstruction, Precambrian Research, 100, 21-63, 2000.

Preiss, W. V.: The tectonic history of Adelaide's scarp-forming faults, Australian Journal of Earth Sciences, 66, 305-365,
645 10.1080/08120099.2018.1546228, 2019.

Reid, A. and Forster, M., 2021, Complex 40Ar/39Ar age spectra from low metamorphic grade rocks, Delamerian Orogen, Reid et al, Mendeley Data, V1, doi: 10.17632/g75hgmypbw.1

Renne, P. R., Mundil, R., Balco, G., Min, K., and Ludwig, K. R.: Joint determination of 40K decay constants and 40Ar∗/40K for the Fish Canyon sanidine standard, and improved accuracy for 40Ar/39Ar geochronology, Geochimica et Cosmochimica
650 Acta, 74, 5349-5367, 10.1016/j.gca.2010.06.017, 2010.

Schodlok, M. C., Whitbourn, L., Huntington, J., Mason, P., Green, A., Berman, M., Coward, D., Connor, P., Wright, W., Jolivet, M., and Martinez, R.: HyLogger-3, a visible to shortwave and thermal infrared reflectance spectrometer system for drill core logging: functional description, Australian Journal of Earth Sciences, 63, 929-940, 10.1080/08120099.2016.1231133, 2016.

655 Stuart, F. M.: The exhumation history of orogenic belts from 40Ar/39Ar ages of detrital micas, Mineralogical Magazine, 66, 121-135, 10.1180/0026461026610017, 2002.

Tetley, N., McDougall, I., and Heydegger, H. R.: Thermal neutron interferences in the 40Ar/39Ar dating technique, Journal of Geophysical Research: Solid Earth, 85, 7201-7205, https://doi.org/10.1029/JB085iB12p07201, 1980.

Turner, S. P., Kelley, S. P., VandenBerg, A. H. M., Foden, J. D., Sandiford, M., and Flöttmann, T.: Source of the Lachlan fold
660 belt flysch linked to convective removal of the lithospheric mantle and rapid exhumation of the Delamerian-Ross fold belt, Geology, 24, 941-944, 10.1130/0091-7613(1996)024<0941:sotlfb>2.3.co;2, 1996.

Wijbrans, J. R. and McDougall, I.: Metamorphic evolution of the Attic Cycladic Metamorphic Belt on Naxos (Cyclades, Greece) utilizing 40Ar/39Ar age spectrum measurements, Journal of Metamorphic Geology, 6, 571-594, https://doi.org/10.1111/j.1525-1314.1988.tb00441.x, 1988.

665 Zack, T. and Hogmalm, K. J.: Laser ablation Rb/Sr dating by online chemical separation of Rb and Sr in an oxygen-filled reaction cell, Chemical Geology, 437, 120-133, https://doi.org/10.1016/j.chemgeo.2016.05.027, 2016.